Bubble Behaviors in a Slowly Rotating Helium Dewar in a Gravity Probe-B Spacecraft Experiment

R. J. Hung,* Y. D. Tsao,† and B. B. Hong‡
University of Alabama in Huntsville, Huntsville, Alabama
and
Fred W. Leslie§
NASA Marshall Space Flight Center, Huntsville, Alabama

Potential problems for the Gravity Probe-B (GP-B) spacecraft design requirements and the operational considerations could arise because of the free surface configurations between liquid helium and helium vapor in the rotating dewar. This free surface is present in the partially filled liquid helium dewar. The liquid helium in the dewar is depleted as it is consumed as propellant for the spacecraft. In this study, the doughnut-shaped helium bubble equilibrium profiles in the rotating dewar have been numerically calculated. These calculations were performed under the conditions imposed during the period of the GP-B experiment instrument calibration (gyro spinup period) and also during the normal operational stages of the GP-B spacecraft.

Nomenclature

A = defined by Eqs. (10), (12), (14), (16), (18), and (20)
$f(r)$ = defined by Eqs. (9), (11), (13), (15), (17), and (19)
$\hat{n}_0$ = unit normal vector pointing outward from the surface
P = fluid pressure
r = radial axis in cylindrical coordinates
r_0 = radius of bubble intersecting the wall
R_1^{-1} = defined by Eq. (5)
R_2^{-1} = defined by Eq. (6)
R_1 = inner radius of dewar
R_2 = outer radius of dewar
R_M = maximum radius of bubble
R_0 = radius of highest or lowest boundary of bubble
z = axial (height) axis in cylindrical coordinates
∇ = divergent (vector) operator
θ = contact angle
ρ = density
σ = coefficient of surface tension
ϕ = dz/dr
ψ = $A/\sigma r$

Subscripts

u = upper region
L = lower region
i = inside the interface
o = outside the interface

Superscripts

L = left-hand side of the bubble region
R = right-hand side of the bubble region
i = inside the interface
o = outside the interface

I. Introduction

THE Gravity Probe-B (GP-B) spacecraft (see Fig. 1) is designed to test the general theory of relativity through long-term (1-yr) monitoring the precession of a set of gyros in free-fall around the Earth.[1,2] Extraneous forces on these gyros must be kept at very low levels, corresponding to an acceleration of 10^{-10} g or less. This will require a drag-free (to 10^{-10} g) control system that uses a proof mass similar to the experiment gyros as its sensing element. The experiment uses superconducting sensors for gyro readout and maintains a very low temperature for mechanical stability. The approaches to both cooling and control involve the use of superfluid liquid helium. The boil-off from the liquid helium dewar (Fig. 2) will be used as a propellant to maintain the altitude control and drag-free operation of the spacecraft. The requirement for an operational lifetime approaching 1 yr means that a large quantity of liquid helium must be used and that it will be gradually depleted over the lifetime of the experiment. This varying amount of liquid helium gives rise to the possibility of several problems that can degrade the GP-B experiment. The potential problems could be the result of asymmetry in the static liquid helium distribution or perturbations in the free surface.

In a study of the attraction of unsymmetric liquid helium distributions on the proof mass, Schafer and Lowry[3] showed that, with liquid helium on one side in a half-full dewar, the resulting acceleration levels at the proof mass are about 10^{-8} g. In the absence of temperature gradient along the surface that drives Maragoni convection, the equilibrium shape of a free surface is governed by a balance of capillary, centrifugal, and gravitational forces. In contrasting the effects of surface tension to the effects of gravitational forces on the free surface of liquid, it was found that the surface tension force for most liquids is greater than the gravitational force in a 10^{-8} g level and lower.[4-6] In other words, the equilibrium shape of the liquid helium free surface in the operational GP-B spacecraft is

Received June 3, 1988; revision received Sept. 26, 1988.

*Professor, Department of Mechanical Engineering. Associate Fellow AIAA.
†Research Engineer, Department of Mechanical Engineering.
‡Graduate Student, Department of Mechanical Engineering.
§Chief, Fluid Dynamics Branch.

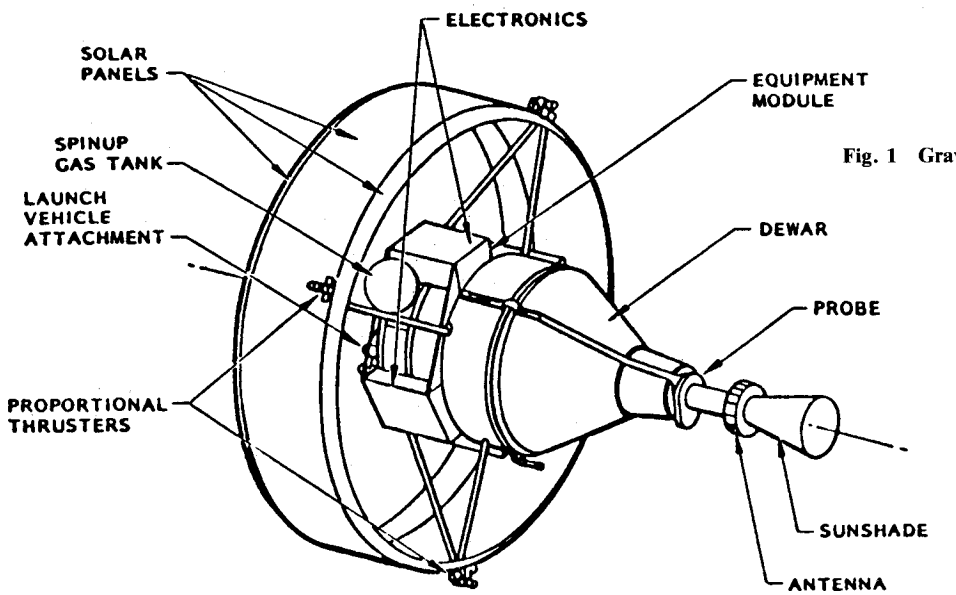

Fig. 1 Gravity Probe-B spacecraft conceptual design.

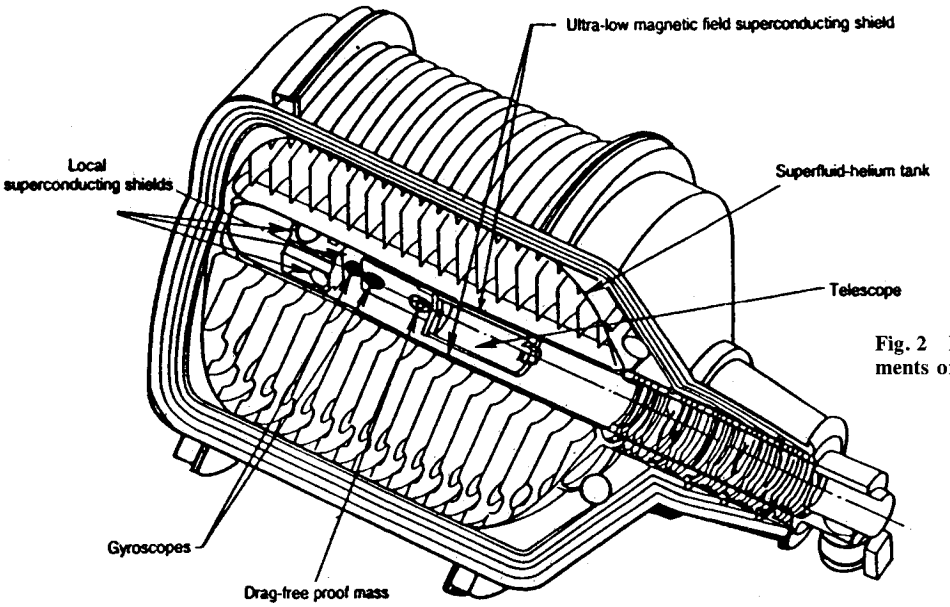

Fig. 2 Experiment GP-B module showing main elements of the liquid helium dewar and probe.

governed by a balance of capillary and centrifugal forces, instead of a balance of capillary, centrifugal, and gravitational forces. Therefore, one may ignore the effect of gravitational force in the gravity environment levels of 10^{-8} g and lower in comparison to the surface tension force. Determination of bubble profiles based on computational experiments can uncover details of the flow that cannot be easily visualized or measured experimentally.[7-10]

For the GP-B spacecraft liquid helium management problem, the geometries are so large that the critical values of superfluid are exceeded. The experiments carried out by Mason et al.[11] showed that the classical fluid mechanics theory is applicable for liquid helium in large containers.

In this paper, the equilibrium configurations of the helium bubble in a rotating dewar have been studied. They are relevant to the questions of fluid behavior in a microgravity environment that were raised by design and operational considerations for the GP-B experiment. For a spacecraft operating as designed, spacecraft drag will be balanced by the helium propulsion system. There should be no net acceleration, above the 10^{-10} g level, on the liquid helium from these sources. However, Schafer and Lowry[3] pointed out that liquid helium mass distributions in the GP-B dewar are possible that are capable of producing accelerations on the proof mass on the order of 10^{-8} g. Our earlier studies[4-6] showed that the gravitational force of 10^{-8} g level and lower will never affect the equilibrium shape of the liquid helium free surface because the effect of the surface tension force is overwhelmingly greater than that of the gravitational force at these levels.

As to the effect of centrifugal force on the helium bubble, the dewar will not be spinning when the GP-B spacecraft is deployed. In the early stages of the experiment, a spin rate of up to about 1 rpm will be imposed for instrument calibration. After calibration, the rotation rate will be reduced to its operational value of approximately 0.1 rpm.

Helium bubble equilibrium profiles in a rotating dewar, within the operational conditions of GP-B spacecraft, have been considered for the following two cases: 1) low rotating speed, from 10^{-3} to 0.15 rpm and 2) high rotating speed, from 0.2 to 10 rpm, in microgravity levels.

II. Mathematical Model

The evaporation of helium vapor makes a two-phase fluid rotating inside the gyro-probe dewar. The geometry of a rotating free surface between helium vapor (vapor bubble) and liquid helium, under a microgravity environment, can be classified into the following two categories: 1) bubble intersecting the inner vertical wall of the dewar (low rotating speed)

(see Fig. 3) and 2) bubble intersecting the top and bottom walls of the dewar (high rotating speed) (see Fig. 4).

Bubble Intersecting the Inner Vertical Wall of the Dewar (Low Rotating Speed in a Microgravity Environment)

At the surface of two fluids (helium vapor and liquid helium), the pressure discontinuity is governed by Laplace's formula:

$$P^i - P^o = \sigma \nabla \cdot \hat{n}_0 \tag{1}$$

where P^i denotes pressure inside the bubble and P^o the pressure outside the bubble.

In general, P^i and P^o are determined from the full set of Navier-Stokes equations. For the special case of a steady-state rotating fluid, with the assumption of axial symmetry, P^i and P^o can be easily determined analytically from the Navier-Stokes equations. The solutions in cylindrical coordinates are given by

$$P^i = P^i_o + \tfrac{1}{2}\rho_i \omega^2 r^2 - \rho_i g z \tag{2}$$

$$P^o = P^o_o + \tfrac{1}{2}\rho_0 \omega^2 r^2 - \rho_0 g z \tag{3}$$

where ρ is the density of fluid; g, the gravitational acceleration; and the subscripts or superscripts i and o denote physical parameters inside (such as internal pressure) and outside (such as external pressure) of the interface, respectively.

For the case of axial symmetry, the gradient of n_0 can be further written as

$$\nabla \cdot \hat{n}_0 = R_1^{-1} + R_2^{-1} \tag{4}$$

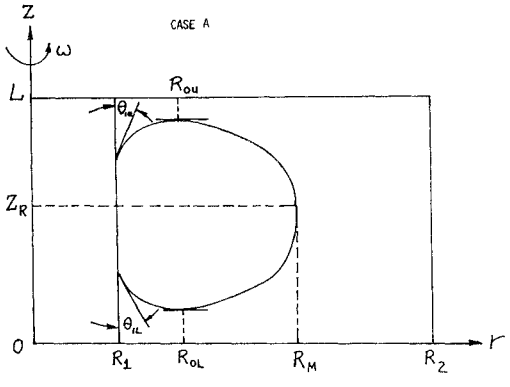

Fig. 3 Definition of the cylindrical coordinate system for the free surface of helium bubble with low-rotating-speed dewar in a low-gravity level used for the analytical model.

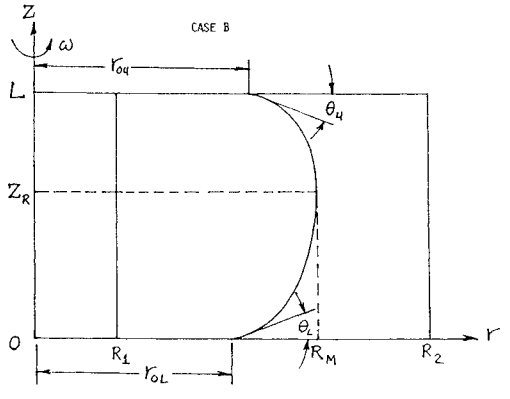

Fig. 4 Definition of the cylindrical coordinate system for the free surface of helium bubble with high-rotating-speed dewar in a low gravity level used for the analytical model.

where

$$R_1^{-1} = \frac{d^2z}{dr^2}\left[1 + \left(\frac{dz}{dr}\right)^2\right]^{-3/2} \tag{5a}$$

$$R_2^{-1} = \frac{dz}{dr} r^{-1}\left[1 + \left(\frac{dz}{dr}\right)^2\right]^{-1/2} \tag{5b}$$

Now, let the profile of the interface be given by $z = f(r)$, and define the following parameters:

$$\phi = \frac{dz}{dr} = \frac{df}{dr} \quad \text{and} \quad \phi' = \frac{d\phi}{dr} = \frac{d^2z}{dr^2}$$

Equation (4) can be rewritten in the form

$$\nabla \cdot \hat{n}_0 = \mp \frac{1}{r}\frac{d}{dr}\left[\frac{r\phi}{(1+\phi^2)^{1/2}}\right] \tag{6}$$

where the upper (lower) sign must be taken if the center of curvature remains to the left (right) of the interface[12] (see Figs. 3 and 4).

Substituting Eqs. (2-4) in Eq. (1) leads to

$$P_o r + \frac{1}{2}\rho\omega^2 r^3 - \rho g z r = \mp\sigma \frac{d}{dr}\left[\frac{r\phi}{(1+\phi^2)^{1/2}}\right] \tag{7}$$

where $P_o = P^i_o - P^o_o$ and $\rho = \rho_i - \rho_o$. Integrating Eq. (7) leads to

$$\frac{1}{2}P_o r^2 + \frac{1}{8}\rho\omega^2 r^4 - \rho g \int rz\, dr = \mp \frac{\sigma r\phi}{(1+\phi^2)^{1/2}} + C \tag{8}$$

Both constant C and the value of P_o can be determined from the boundary conditions illustrated in Figs. 3 and 4. Detailed approaches of the mathematical derivations for the equilibrium profiles of the bubble shapes for the rotating dewar are similar to those of the bubble shapes for a rotating cylinder that were shown in the work of Hung and Leslie[4] and Hung et al.[5] However, the mathematical results are quite different.

The results of the mathematical derivations are given as follows:

Upper Region: $L \geq z \geq z_R$

Left-hand side, upper region (see Fig. 3). For the case of the left-hand side of the upper region, the bubble profile of interface can be obtained from the following integration:

$$z^L_u = f^L_u(r) = \int_{R_1}^{r} \frac{\psi^L_u}{[1-(\psi^L_u)^2]^{1/2}}\, dr \tag{9}$$

where

$$\psi^L_u = A^L_u / \sigma r$$

and

$$A^L_u = -\left(\frac{r^2 - R_1^2}{R_{0u}^2 - R_1^2}\right)\left[\frac{1}{8}\rho\omega^2(R_{0u}^4 - R_1^4) + \rho g \int_{R_{0u}}^{R_1} rz\, dr + \sigma R_1 \cos\theta_{1u}\right] + \frac{1}{8}\rho\omega^2(r^4 - R_1^4) + \rho g \int_r^{R_1} rz\, dr + \sigma R_1 \cos\theta_{1u} \tag{10}$$

Right-hand side, upper region. For the case of the right-hand side of the upper region, the bubble profile of interface can be obtained from the following integration:

$$z^R_u = f^R_u(r) = \int_{R_{0u}}^{r} \frac{\psi^R_u}{[1-(\psi^R_u)^2]^{1/2}}\, dr \tag{11}$$

where

$$\psi_u^R = A_u^R/\sigma r$$

and

$$A_u^R = -\left(\frac{r^2 - R_{0u}^2}{R_M^2 - R_{0u}^2}\right)\left[\frac{1}{8}\rho\omega^2(R_M^4 - R_{0u}^4) + \rho g\int_{R_M}^{R_{0u}} rz\,\mathrm{d}r + \sigma R_M\right] + \frac{1}{8}\rho\omega^2(r^4 - R_{0u}^4) + \rho g\int_r^{R_{0u}} rz\,\mathrm{d}r \tag{12}$$

Lower Region: $z_R > z \geq 0$

Left-hand side, lower region. For the case of the left-hand side of the lower region, the bubble profile of interface can be obtained from the following integration:

$$z_L^L = f_L^L(r) = \int_{R_1}^{r} \frac{\psi_L^L}{[1-(\psi_L^L)^2]^{1/2}}\,\mathrm{d}r \tag{13}$$

where

$$z_L^L = z < z_R$$

$$\psi_L^L = A_L^L/\sigma r$$

and

$$A_L^L = -\left(\frac{r^2 - R_1^2}{R_{0L}^2 - R_1^2}\right)\left[\frac{1}{8}\rho\omega^2(R_{0L}^4 - R_1^4) - \rho g\int_{R_1}^{R_{0L}} rz\,\mathrm{d}r - \sigma R_1\cos\theta_{1L}\right] + \frac{1}{8}\rho\omega^2(r^4 - R_1^4) - \rho g\int_{R_1}^{r} rz\,\mathrm{d}r - \sigma R_1\cos\theta_{1L} \tag{14}$$

Right-hand side, lower region. For the case of the right-hand side of the lower region, the bubble profile of interface can be obtained from the following integration:

$$z_L^R = f_L^R(r) = \int_{R_{0L}}^{r} \frac{\psi_L^R}{[1-(\psi_L^R)^2]^{1/2}}\,\mathrm{d}r \tag{15}$$

where

$$z_L^R = z < z_R$$

$$\psi_L^R = A_L^R/\sigma r$$

and

$$A_L^R = -\left(\frac{r^2 - R_M^2}{R_{0L}^2 - R_M^2}\right)\left[\frac{1}{8}\rho\omega^2(R_{0L}^4 - R_M^4) + \rho g\int_{R_{0L}}^{R_M} rz\,\mathrm{d}r + \frac{1}{8}\rho\omega^2(r^4 - R_M^4) + \rho g\int_r^{R_M} rz\,\mathrm{d}z\right] \tag{16}$$

Bubble Intersecting Upper and Lower Walls of the Dewar (see Fig. 4)

Upper Region: $L \geq z \geq z_R$

For the case of the upper region, the bubble profile of interface can be obtained from the following integration:

$$z_u = f_u(r) = \int_{r_{0u}}^{r} \frac{\psi_u}{(1-\psi_u^2)^{1/2}}\,\mathrm{d}r \tag{17}$$

where

$$z_u = z > z_R$$

$$\psi_u = A_u/\sigma r$$

and

$$A_u = -\left(\frac{r^2 - r_{0u}^2}{R_M^2 - r_{0u}^2}\right)\left[\frac{1}{8}\rho\omega^2(R_M^4 - r_{0u}^4) - \rho g\int_{r_{0u}}^{R_M} rz\,\mathrm{d}r + \sigma(R_M + r_{0u}\sin\theta_u)\right] + \frac{1}{8}\rho\omega^2(r^4 - r_{0u}^4) - \rho g\int_{r_{0u}}^{r} rz\,\mathrm{d}r + \sigma r_{0u}\sin\theta_u \tag{18}$$

Lower Region: $z_R > z \geq 0$

For the case of the lower region, the bubble profile of interface can be obtained from the following integration:

$$z_L = f_L(r) = \int_{r_{0L}}^{r} \frac{\psi_L}{(1-\psi_L^2)^{1/2}}\,\mathrm{d}r \tag{19}$$

where

$$z_L = z < z_R$$

$$\psi_L = A_L/\sigma r$$

and

$$A_L = -\left(\frac{r^2 - r_{0L}^2}{R_M^2 - r_{0L}^2}\right)\left[\frac{1}{8}\rho\omega^2(R_M^4 - r_{0L}^4) - \rho g\int_{r_{0L}}^{R_M} rz\,\mathrm{d}r + \sigma(R_M + r_{0L}\sin\theta_L)\right] + \frac{1}{8}\rho\omega^2(r^4 - r_{0L}^4) - \rho g\int_{r_{0L}}^{r} rz\,\mathrm{d}r - \sigma r_{0L}\sin\theta_L \tag{20}$$

III. Numerical Calculation of Equilibrium Profiles of Helium Bubble in a Rotating Dewar

Transport coefficients of normal liquid helium were used, since the experimental results[11] show that they have exceeded the critical values of superfluid for the large geometries to be used in the GP-B spacecraft propulsion system. In this study, the following data were used: liquid helium density = 0.145 g/cm^3, helium vapor density = 0.00147 g/cm^3, surface tension between vapor and liquid helium = 0.5 dyne/cm, temperature of liquid helium = 4°K.[13] The computation is based on 90% liquid helium and 10% helium vapor by volume contained in the dewar. The contact angles between liquid helium and the solid walls for all the cases are $\theta = 10$ deg. The size of the dewar is as follows: outer radius = 68 cm, inner radius = 12 cm, and height = 145 cm. In this computation, the gravity gradient at the orbit of the spacecraft is taken into consideration.

The gravity environment in the operational consideration of the GP-B spacecraft is no greater than 10^{-10} g level.[1,2] However, liquid helium mass distributions in the GP-B dewar are capable of producing accelerations on the proof mass on the order of 10^{-8} g, based on the calculations made by Schafer and Lowry,[3] although this is a remote possibility. It has been shown that the gravitational force never affects the equilibrium profiles of the helium bubble if the gravity environment is below the 10^{-7} g level, because the effect of the surface tension force is greater than that of the gravitational force at these levels.

There are only two spin rates for the liquid helium dewar in the GP-B spacecraft: a spin rate of 1 rpm, used for gyro spinup at the beginning, and a 0.1-rpm rotation rate for normal operational conditions. The range of computation for dewar rotation rate covers from 10^{-3} to 10 rpm.

A computer algorithm was developed to integrate two cases of equilibrium bubble profiles of the rotating liquid helium dewar, shown in Figs. 3 and 4. Figures 5a and 5b show the flowcharts for the procedures of computation for numerically

solving these equations shown in Sec. II of the mathematical model of this paper.

As we have discussed in our previous work,[4,5] the calculations were initiated with an estimate of the bubble shape (in this case, doughnut-shaped bubbles with various cross-sectional geometries, as shown in Figs. 3 and 4) for computing a series of the evolution of equilibrium profiles of bubbles depending on the change in the rotating speeds of the dewar.

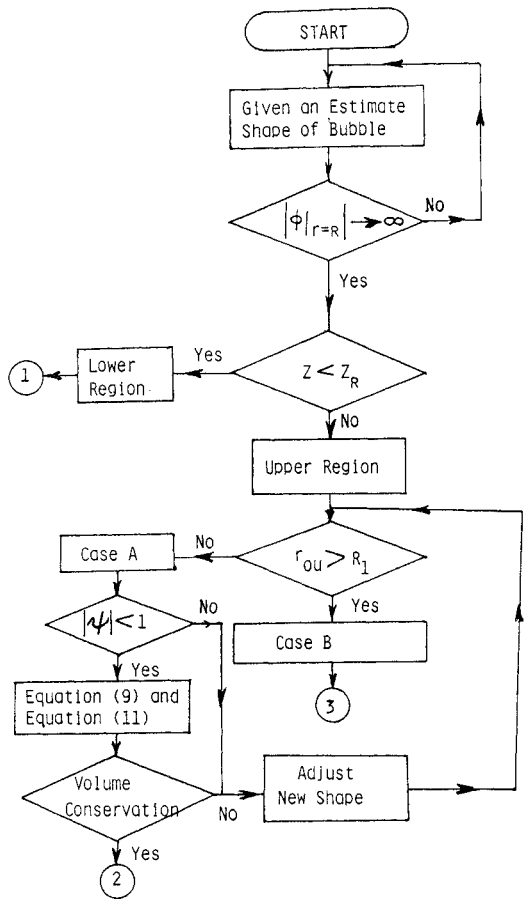

Fig. 5a Flowchart for the procedures of computation for numerically solving Eqs. (9), (11), (19), and (21).

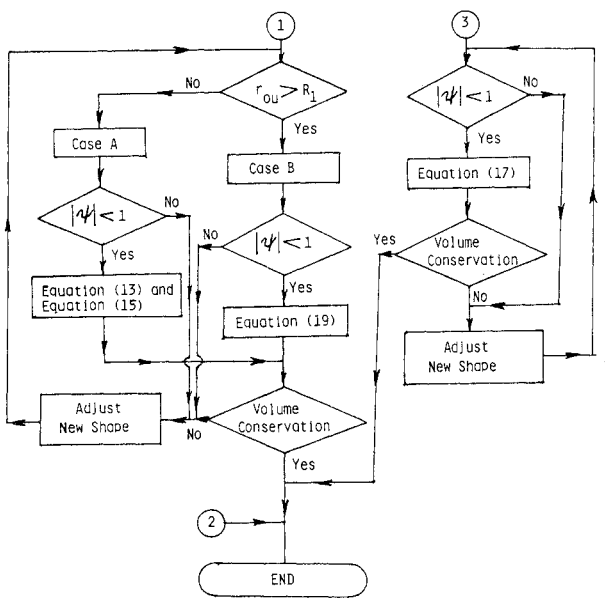

Fig. 5b Flowchart for the procedures of computation for numerically solving Eqs. (15), (17), (23), (25), and (29).

These computations were accomplished through the integral terms in Eqs. (10), (12), (14), (16), (18), and (20). A number of iterations were made to minimize the difference between the trial profile of the bubble shape in the integration of $\int rz\, dz$ in these equations mentioned earlier and the final profile of the bubble shape obtained from the integration of Eqs. (9), (11), (13), (15), (17), and (19). After the integration was complete, the measured volume and computed volume of the bubble were compared. The computed equilibrium profiles of the bubble shapes for the case of a rotating cylinder (in our earlier study[4,5]) have been compared with a series of measurements in the microgravity environment of a free-falling aircraft (KC-135)[7] with excellent agreement.

Numerical calculation shows that, in a gravity environment with the levels of 10^{-7} g and lower, as shown in Figs. 6 and 7, the effect of the gravitational force on the equilibrium shapes of helium vapor bubbles is negligible. There is no difference between the calculated bubble profiles under such a microgravity environment and the calculated bubble profiles under the zero-gravity environment. Figure 6 shows the doughnut-shaped bubble with cross-sectional profile of rotating equilibrium free surfaces in rotating speeds of 10^{-3}, 10^{-2}, 0.1, and 0.15 rpm. Figure 7 illustrates the cross-sectional profile of free surfaces in rotating speeds of 0.2, 0.6, 1.0, and 10 rpm under the gravity environment of 10^{-7} g. The following conclusions can be drawn based on these two figures:

1) A doughnut-shaped helium vapor bubble with a symmetric cross-sectional profile between upper and lower halves occurs for flows in a rotating dewar under the gravity environment of 10^{-7} g and lower.

2) The minimum inner radius of the doughnut-shaped bubble is always contacted to the inner radius of the dewar, and the maximum outer radius of the bubble decreases as the rotating speed increases.

3) The cross-sectional profile of the doughnut-shaped bubble is a circle-like shape when the rotating speed is low and is

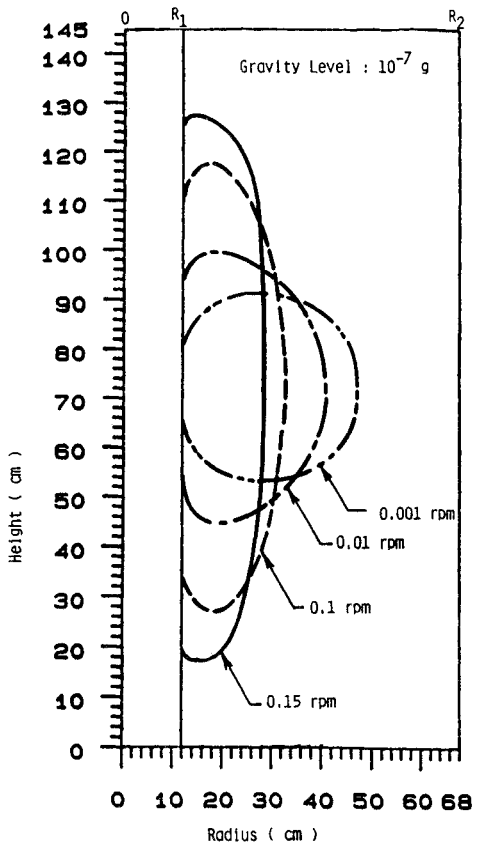

Fig. 6 Cross-sectional profiles of doughnut-shaped helium bubble in a rotating dewar with speeds of 10^{-3}, 10^{-2}, 0.1, and 0.15 rpm in a gravity environment with level of 10^{-7} g and contact angle $\theta = 10$ deg.

elongated along the axis of rotation when the rotating speed increases.

4) As the rotating speed increases and approaches the value of 0.2 rpm, the elongated profile at the upper and lower edges of the doughnut-shaped bubble start to detach from the inner radius of the dewar and contact the upper and lower walls with knife-edge-shaped profiles of free surface near these locations.

5) As the rotating speed increases more and approaches the value of 10 rpm, the knife-edge-shaped free surface near the upper and lower walls or the dewar disappears gradually and the bubble profile eventually becomes a hollow cylinder.

IV. Discussion and Conclusions

In the design of the GP-B spacecraft, there are some strict constraints. The potentaial problems could be the results of asymmetry in the static liquid helium distribution or perturbations in free surface, which is present in the partially filled dewar. In this study, doughnut-shaped helium bubble equilibrium profiles in a rotating dewar under the conditions of low rotating speed (see Fig. 3) and high rotating speed (see Fig. 4) in a microgravity level have been numerically calculated.

Our numerical calculation shows that, for a gravity environment with the levels of 10^{-7} g or lower, the effect of the gravitational force on the equilibrium shapes of the helium vapor bubble is not different from that calculated for a gravity environment with the level of zero gravity. This is required by the design of the GP-B spacecraft experiment to maintain a very-low-gravity environment in the level of 10^{-10} g or less. Figures 6 and 7 show the evolution of doughnut-shaped bubbles in rotating speeds ranging from 10^{-3} to 10 rpm under a gravity environment of 10^{-7} g. Our calculation shows that the doughnut-shaped bubble evolves from a cross-sectional profile of a circle-like shape, to a vertically elongated semicircle, then to a semiellipse, and finally to a hollow cylinder as the rotating speed of the dewar increases from 10^{-3} to 10 rpm.

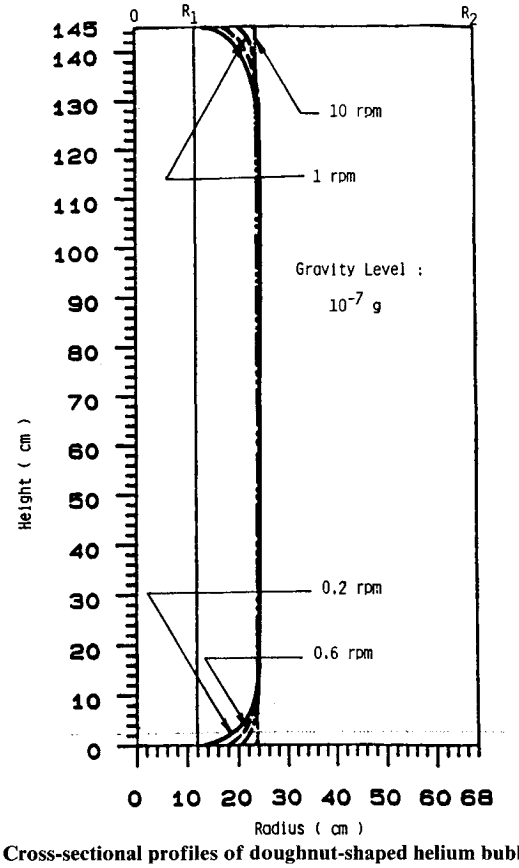

Fig. 7 Cross-sectional profiles of doughnut-shaped helium bubble in a rotating dewar with speeds of 0.2, 0.6, 1.0, and 10 rpm in gravity environment with level of 10^{-7} g and contact angle of $\theta = 10$ deg.

Equilibrium profiles of bubble shapes are determined self-consistently by the balance of capillary, centrifugal, and gravitational forces. In other words, there is no effect on gyros or the proof mass after the equilibrium profile of the bubble shape has been attained.

In the absence of temperature gradient along the surface, which drives Maragoni convection, the equilibrum shape of the free surface is governed by a balance of capillary, centrifugal, and gravitational forces. The role of force fields in the determination of equilibrium bubble profiles, illustrated in Figs. 3 and 4, is different for different cases. The dominating force fields are as follows: 1) low rotating speed in a microgravity level (dominated by surface tension force, as shown in Fig. 3 and 2) high rotating speed in a microgravity level (dominated by a coupling of a centrifugal and surface tension forces as shown in Fig. 4).

In this study, we have demonstrated that the computer algorithm presented can be used to simulate the profile of the doughnut-shaped bubble governed by a balance of capillary and centrifugal forces under microgravity environment.

Acknowledgments

R. J. Hung, Y. D. Tsao, and B. B. Hong appreciate the support received from the NASA Marshall Space Flight Center through NASA Grant NAG8-035. The authors would like to express their gratitude to Richard A. Potter of NASA Marshall Space Flight Center for the stimulating discussion during the course of the present study.

References

[1]Wilkinson, D. T., Bender, D. M., Gaisser, T. K., Harthe, J. B., Israel, M. H., Jones, L. W., Partridge, R. B., Schromm, D. N., Shapiro, I. I., Vessort, R. F. C., and Wagoner, R. V., "Gravitation, Cosmology and Cosmic-Ray Physics," *Physics Today,* Vol. 39, April 1986, pp. 43–46.

[2]"Stanford Relativity Gyroscope Experiment (NASA Gravity Probe B)," *Proceedings of the Society of Photo-Optical Instrumentation Engineers,* Vol. 619, Society of Photo-Optical Instrumentation Engineers, Bellingham, WA, 1986, pp. 1–165.

[3]Schafer, C. F. and Lowry, S. A., "Mechanics of Liquid Helium in a Partially Filled Rotating Dewar in Low Gravity—With Application to Gravity Probe-B," NASA TP-2124, Jan. 1983, p. 38.

[4]Hung, R. J. and Leslie, F. W., "Bubble Shapes in a Liquid-Filled Rotating Container Under Low Gravity," *Journal of Spacecraft and Rockets,* Vol. 25, Jan.-Feb. 1988, pp. 70–74.

[5]Hung, R. J., Tsao, Y. D., Hong, B. B., and Leslie, F. W., "Surface Tension and Bubble Shapes in a Partially Filled Rotating Cylinder Under Low Gravity," AIAA Paper 88-0455, Jan. 1988, p. 9.

[6]Hung, R. J., Tsao, Y. D., Hong, B. B., and Leslie, F. W., "Time Dependent Dynamical Behavior of Surface Tension on Rotating Fluids Under Microgravity Environment," *Advances in Space Research,* Vol. 22, 1988 (to be published).

[7]Leslie, F. W., "Measurements of Rotating Bubble Shapes in a Low Gravity Environment," *Journal of Fluid Mechanics,* Vol. 161, Dec. 1985, pp. 269–279.

[8]Kitchens, C. W., Jr., "Navier-Stokes Equations for Spin-Up in a Filled Cylinder," *AIAA Journal,* Vol. 18, Aug. 1980, pp. 929–934.

[9]Veldman, A. E. P and Vogels, M. E. S., "Axisymmetric Liquid Sloshing Under Low Gravity Conditions," *Acta Astronautica,* Vol. 11, Oct.-Nov.1984, pp. 641–649.

[10]Homicz, G. F. and Gerber, N., "Numerical Model for Fluid Spin-Up from Rest in a Partially Filled Cylinder," *Journal of Fluids Engineering,* Vol. 109, June 1987, pp. 194–197.

[11]Mason, P., Collins, D., Petrae, D., Yang, L., Edeskuty, F., Schuch, A., and Williamson, K., "The Behavior of Superfluid Helium in Zero Gravity," *Proceedings of the 7th International Cryogenic Engineering Conference,* Science and Technology Press, Surrey, England, UK, 1978, pp. 99–112.

[12]Myshkis, A. D., Babskii, V. G., Kopachevskii, N. D., Slobozhanin, L. A., Tyuptsov, A. D., *Low Gravity Fluid Mechanics,* Springer-Verlag, New York, 1987, p. 586.

[13]Weast, R. C. (ed.), *Handbook of Chemistry and Physics,* 50th ed., Chemical Rubber Co., Cleveland, OH, 1980, p. 2454.